STATISTICAL MODELING OF ATTENUATION-CORRECTED PET DATA WITH APPLICATION TO RECONSTRUCTION OF REGIONAL TIME ACTIVITY CURVES

Evgeny Krestyannikov, Jussi Tohka and Ulla Ruotsalainen

Institute of Signal Processing, Tampere University of Technology,
Tampere, P.O.Box 553, FIN-33101, Finland

ABSTRACT

Correction for tissue attenuation is the most important factor affecting the Poisson characteristics of positron emission tomography (PET) data. Although a weighting scheme incorporating the attenuation correction factors in the update rule of expectation-maximization (EM) image reconstruction algorithm has previously been presented [1], no exact distribution of pre-corrected measurements has been proposed to date. This paper introduces a fixed multiplicative Poisson distribution to model the PET data compensated for the effect of photon attenuation. We show that the attenuation-weighted EM update rule can be derived in a formal way via maximizing the log-likelihood of pre-corrected measurements. We use the proposed distribution to develop a joint penalized-likelihood approach for reconstruction of regional time activity curves (TACs) and regions-of-interest from dynamic brain PET projection data. The new method yields lower error in reconstructed TACs compared to the joint reconstruction approach based on ordinary Poisson approximation.

Index Terms: Attenuation, modeling, penalized-likelihood estimation, PET, time activity curve.

1. INTRODUCTION

In quantitative positron emission tomography (PET) the tracer concentration in tissue has to be compensated for the effect of photon attenuation. The correction is typically carried out as a multiplication of the sinogram counts by the respective attenuation correction factors (ACFs). The measured ACF estimates are obtained from the transmission data recorded using the external positron sources, γ-ray sources, or X-ray sources on the integrated PET/computed tomography (CT) systems [2].

The multiplication of the Poisson random variable by the ACF alters the statistical properties of the distribution causing excess fluctuations with variance significantly exceeding the count mean. It has been shown that the use of iterative maximum-likelihood reconstruction algorithms (e.g. ordered subsets expectation - maximization (OSEM)) yields images with poor noise-bias trade-off from such data [3]. An alternative strategy is to apply iterative reconstruction algorithms to the data with restored Poisson statistics. This kind of data decorrection is typically done via incorporating the ACFs to the system matrix [1, 3].

In this paper, we provide an exact two-parameter distribution of the attenuation-corrected emission data referred to as the fixed multiplicative Poisson distribution. It gives a good description for the counting of photons generated by random Poisson process amplified by some constant multiplicative factor. We present analytical expressions for the probability mass function, first-, and second-order moments. The exact log-likelihood function of the pre-corrected measurements is tractable, that enables its direct maximization. In the following section, we show that the attenuation-weighted EM image reconstruction algorithm [1] can be derived in a formal way by maximizing the fixed multiplicative Poisson log-likelihood.

Explicit statistical modeling of photon counting data pre- corrected for attenuation (and for multiplicative factors, in general) can be particularly useful in situations where the use of correction factors separately from the data is not feasible. We apply the proposed fixed multiplicative Poisson distribution for region-of-interest (ROI) quantification in dynamic PET. We present a method for joint penalized-likelihood reconstruction of time activity curves (TACs) and ROIs from pre-corrected projection data. The method is able to refine the TAC estimates even if an accurate partitioning of image into ROIs is not available. We modify our recently developed joint penalized-likelihood estimator which is based on ordinary Poisson approximation [4] to account for the effect of photon attenuation. On a numerical phantom with simulated attenuation correction, we show that the modified scheme yields lower error for TAC estimates.

2. STATISTICAL MODEL FOR THE ATTENUATION-CORRECTED SINOGRAM DATA

We assume that for each voxel $i = 1, \ldots, I$ at time interval $t = 1, \ldots, T$ the radioactive decay process generates random number of photons X_{it} drawn from the Poisson distribution with the mean λ_{it}. Transmission of photons through the body

Supported by Tampere Graduate School in Information Technology (TISE); the Academy of Finland under the Grants No. 108517, 104834, and 213462 (Finnish Centre of Excellence Programme 2006-2011).

is characterized by the linear attenuation coefficient at voxel position i. The number of photons G_{dt} not interacted with the tissue and recorded by the detector $d = 1, \ldots, D$ are conditionally independent according to the Poisson distribution with the mean

$$\nu_{dt} = \sum_i \left(p_{di} e^{-\mu_d} \right) \lambda_{it}. \quad (1)$$

The factor p_{di} is the conditional probability that a photon pair emitted at ith voxel was counted by dth detector pair, μ_d is the integral of attenuation coefficients along the line of response (LOR) d. The term $e^{-\mu_d}$ is the survival probability that the two photons generate a count at detector pair d.

To account for the effect of attenuation, the *a posteriori* weighting is performed as

$$\hat{G}_{dt} = e^{\mu_d} G_{dt} = a_d G_{dt}, \quad (2)$$

where a_d is the multiplicative ACF. Let g_{dt} and $\hat{g}_{dt}$ be realizations of statistically independent random variables G_{dt} and $\hat{G}_{dt}$, respectively. Under the assumption about independence between different rays, the exact distribution of $\hat{g}_{dt}$ can be expressed using the total probability as

$$\begin{aligned} p(\hat{g}_{dt}; \nu_{dt}) &= \sum_{g_{dt}=0}^{\infty} p(\hat{g}_{dt}|g_{dt}) p(g_{dt}|\nu_{dt}) \\ &= \sum_{g_{dt}=0}^{\infty} \delta\left(\frac{\hat{g}_{dt}}{a_d} - g_{dt} \right) \left(\frac{\nu_{dt}^{g_{dt}} e^{-\nu_{dt}}}{g_{dt}!} \right) \\ &= \frac{\nu_{dt}^{\hat{g}_{dt}/a_d} e^{-\nu_{dt}}}{(\hat{g}_{dt}/a_d)!}, \end{aligned} \quad (3)$$

where $\delta(\cdot)$ is the delta function. The above distribution was introduced by Teich [5] under the name of fixed multiplicative Poisson distribution to describe the multiplied Poisson processes in photon counting. Its mean and variance are

$$E(\hat{G}_{dt}) = a_d \nu_{dt}, \quad (4)$$

$$\mathrm{var}(\hat{G}_{dt}) = a_d^2 \nu_{dt}. \quad (5)$$

Given the parametric form (1) for ν_{dt}, the exact log-likelihood of the unknown image $\boldsymbol{\lambda}_t$ at time interval t becomes

$$L(\boldsymbol{\lambda}_t) = \sum_d \left[-\frac{\sum_i p_{di} \lambda_{it}}{a_d} + \frac{\hat{g}_{dt}}{a_d} \log \left(\frac{\sum_i p_{di} \lambda_{it}}{a_d} \right) \right]. \quad (6)$$

Utilizing the optimization transfer principles (in a similar way as in [6]), it is easy to verify that the maximization of (6) yields an update equation in the attenuation-weighted EM algorithm [1 eq(5)]

$$\lambda_{it}^{(j+1)} = \frac{\lambda_{it}^{(j)}}{\sum_d p_{di}/a_d} \sum_d \left(\frac{\hat{g}_{dt} p_{di}}{a_d \sum_{i'} p_{di'} \lambda_{i't}^{(j)}} \right). \quad (7)$$

3. RECONSTRUCTION OF REGIONAL TACS FROM ATTENUATION-CORRECTED DATA

3.1. Joint penalized log-likelihood

We assume that the whole field of view can be partitioned into a set regions with homogeneous activity concentration $\Omega_k, k = 1, 2, \ldots, K$ of arbitrary shape, such that within each region a single TAC can fully describe the tracer's behavior. The equation (1) can be then rewritten as

$$\nu_{dt} = \sum_k \left(b_{dk} e^{-\mu_d} \right) \lambda_{kt}, \quad (8)$$

where $\lambda_{kt} = \lambda_{it}, \forall i \in \Omega_k$ is the mean radioactivity quantified within kth ROI at time interval t. The element b_{dk} is the unnormalized conditional probability that a photon pair emitted at tissue k was counted by detector d. It relates to factors p_{di} through $b_{dk} = \sum_{i \in \Omega_k} p_{di}$. The kth column of matrix $\mathbf{B}$ represents a projection of the kth spatial ROI. The ROI can be a binary labelled image if the partial volume effect is not taken into consideration, or a fuzzy labelled image which models the fraction of kth tissue type present in each particular voxel. The estimation problem is to infer both the unknown TACs and the matrix of ROI projections from the pre-corrected count data.

Given (8), the joint log-likelihood of parameters $\boldsymbol{\lambda}$ and $\mathbf{B}$ becomes

$$L(\boldsymbol{\lambda}, \mathbf{B}) = \sum_{d,t} \left[-\frac{\sum_k b_{dk} \lambda_{kt}}{a_d} + \frac{\hat{g}_{dt}}{a_d} \log \left(\frac{\sum_k b_{dk} \lambda_{kt}}{a_d} \right) \right]. \quad (9)$$

We abbreviate the log-likelihood in (9) as $\sum_{d,t} h_{dt}(l(\boldsymbol{\lambda}, \mathbf{B}))$, where $h_{dt}(l) = -l/a_d + \hat{g}_{dt}/a_d \log(l/a_d)$ and $l(\boldsymbol{\lambda}, \mathbf{B}) = \sum_k b_{dk} \lambda_{kt}$. To assure the identifiability of parameters and to maintain the feasibility of the solution, we impose constraints on rows and columns of matrix $\mathbf{B}$. We realize them via following quadratic penalty functions [4]

$$C_1(\mathbf{B}) = \sum_d \beta_d \left(\frac{\sum_k b_{dk}}{b_d^{\mathrm{mask}}} - 1 \right)^2, \quad (10)$$

$$C_2(\mathbf{B}) = \sum_k \gamma_k \left(\frac{\sum_d b_{dk}}{b_k^{\mathrm{vol}}} - 1 \right)^2. \quad (11)$$

The first penalty term C_1 implements a geometric constraint which ensures that all the spatial ROIs corresponding to different tissue types are enclosed within the reference mask. The element b_d^{mask} is the projection of a binary mask along the LOR corresponding to the detector pair d. The reference brain mask can be delineated beforehand using any surface extraction technique. The second term C_2 alters the initial sinogram volume of different structures towards the predefined values b_k^{vol}. The average proportions of structures of different tissue

type can be computed, for example, based on probabilistic atlases of brain anatomy. The cost for each constraint can be changed by varying the regularization parameters β_d and γ_k. A penalized maximum-likelihood (PML) estimate of $\{\boldsymbol{\lambda}, \mathbf{B}\}$ is obtained then by finding the following maximizer

$$\{\hat{\boldsymbol{\lambda}}, \hat{\mathbf{B}}\} \quad = \quad \arg\max_{\boldsymbol{\lambda},\mathbf{B}} \Psi(\boldsymbol{\lambda}, \mathbf{B}), \tag{12}$$

where

$$\Psi(\boldsymbol{\lambda}, \mathbf{B}) = L(\boldsymbol{\lambda}, \mathbf{B}) - C_1(\mathbf{B}) - C_2(\mathbf{B}). \tag{13}$$

Function Ψ is concave for parameter $\boldsymbol{\lambda}$ if $\mathbf{B}$ is known and vice versa. When both $\boldsymbol{\lambda}$ and $\mathbf{B}$ are unknown, the function Ψ is nonconcave.

3.2. Alternating maximization using EM algorithm

In this section, we propose a method for successive optimization of function Ψ to at least a local maximum by alternately updating $\boldsymbol{\lambda}$ and $\mathbf{B}$. Holding $\mathbf{B}^{(j)}$ fixed on current iteration j, we update the parameter $\boldsymbol{\lambda}$ as

$$\boldsymbol{\lambda}^{(j+1)} = \arg\max_{\boldsymbol{\lambda}} \Psi(\boldsymbol{\lambda}, \mathbf{B}^{(j)}). \tag{14}$$

Similarly, we update $\mathbf{B}$ holding $\boldsymbol{\lambda}^{(j+1)}$ constant as

$$\mathbf{B}^{(j+1)} = \arg\max_{\mathbf{B}} \Psi(\boldsymbol{\lambda}^{(j+1)}, \mathbf{B}). \tag{15}$$

Analytical maximizers to (14)-(15) do not exist due to coupling of variables in L, C_1, and C_2. We develop an EM algorithm to transfer the maximization from Ψ to a separable surrogate function Q which is easier to optimize. Letting $g_{dt}^{(j)} = \sum_k b_{dk}^{(j)} \lambda_{kt}^{(j)}$ and applying the following inequalities due to De Pierro [6, 7]

$$h_{dt}\Big(\sum_k b_{dk}^{(j)} \lambda_{kt}\Big) \geq \sum_k \left(\frac{b_{dk}^{(j)} \lambda_{kt}^{(j)}}{g_{dt}^{(j)}}\right) h_{dt}\left(\frac{g_{dt}^{(j)} \lambda_{kt}}{\lambda_{kt}^{(j)}}\right),$$

$$h_{dt}\Big(\sum_k b_{dk} \lambda_{kt}^{(j+1)}\Big) \geq \sum_k \left(\frac{b_{dk}^{(j)} \lambda_{kt}^{(j)}}{g_{dt}^{(j)}}\right) h_{dt}\left(\frac{g_{dt}^{(j)} b_{dk} \lambda_{kt}^{(j+1)}}{b_{dk}^{(j)} \lambda_{kt}^{(j)}}\right),$$

$$\left(\frac{\sum_k b_{dk}}{b_d^{\text{mask}}} - 1\right)^2 \leq \sum_k \alpha_{dk} \left(\frac{b_{dk} - b_{dk}^{(j)}}{\alpha_{dk} b_d^{\text{mask}}} + \frac{\sum_k b_{dk}^{(j)}}{b_d^{\text{mask}}} - 1\right)^2,$$

$$\left(\frac{\sum_d b_{dk}}{b_k^{\text{vol}}} - 1\right)^2 \leq \sum_d \omega_{dk} \left(\frac{b_{dk} - b_{dk}^{(j)}}{\omega_{dk} b_k^{\text{vol}}} + \frac{\sum_d b_{dk}^{(j)}}{b_k^{\text{vol}}} - 1\right)^2,$$

where $\alpha_{dk}, \omega_{dk} \geq 0, \sum_k \alpha_{dk} = 1, \forall d = 1, \ldots, D; \sum_d \omega_{dk} = 1, \forall k = 1, \ldots, K$, we construct during the E-step the overall separable monotonic surrogate functions $Q(\boldsymbol{\lambda}, \mathbf{B}^{(j)}; \boldsymbol{\lambda}^{(j)}, \mathbf{B}^{(j)})$ and $Q(\boldsymbol{\lambda}^{(j+1)}, \mathbf{B}; \boldsymbol{\lambda}^{(j)}, \mathbf{B}^{(j)})$ for $\Psi(\boldsymbol{\lambda}, \mathbf{B}^{(j)})$ and $\Psi(\boldsymbol{\lambda}^{(j+1)}, \mathbf{B})$, respectively. The maximization of surrogates during the M-step yields the following update rules

$$\lambda_{kt}^{(j+1)} = \frac{\lambda_{kt}^{(j)}}{\sum_d b_{dk}^{(j)} / a_d} \sum_d \left(\frac{\hat{g}_{dt} b_{dk}^{(j)}}{a_d \sum_{k'} b_{dk'}^{(j)} \lambda_{k't}^{(j)}}\right), \tag{16}$$

$$b_{dk}^{(j+1)} = \frac{-E_{dk}/2 + \sqrt{E_{dk}^2/4 - A_{dk} F_{dk}}}{A_{dk}}, \tag{17}$$

where

$$A_{dk} = \frac{\beta_d}{\alpha_{dk} (b_d^{\text{mask}})^2} + \frac{\gamma_k}{\omega_{dk} (b_k^{\text{vol}})^2}, \tag{18}$$

$$\begin{aligned} E_{dk} \quad &= \quad \frac{\sum_t \lambda_{kt}^{(j+1)}}{a_d} - \frac{\beta_d}{b_d^{\text{mask}}} \left(\frac{b_{dk}^{(j)}}{\alpha_{dk} b_d^{\text{mask}}} - \frac{\sum_k b_{dk}^{(j)}}{b_d^{\text{mask}}} + 1\right) \\ &- \quad \frac{\gamma_k}{b_k^{\text{vol}}} \left(\frac{b_{dk}^{(j)}}{\omega_{dk} b_k^{\text{vol}}} - \frac{\sum_d b_{dk}^{(j)}}{b_k^{\text{vol}}} + 1\right), \end{aligned} \tag{19}$$

$$F_{dk} = -b_{dk}^{(j)} \sum_t \left(\frac{\hat{g}_{dt} \lambda_{kt}^{(j)}}{a_d \sum_{k'} b_{dk'}^{(j)} \lambda_{k't}^{(j)}}\right). \tag{20}$$

Due to monotonicity of the overall surrogate, the EM algorithm is guaranteed to monotonically increase Ψ at each iteration.

4. EXPERIMENTAL RESULTS

We validated the statistical model and evaluated the modified PML-EM algorithm with simulated low count dynamic ^{18}F-FDG study. The numerical phantom was derived from the labelled anatomical Zubal phantom and consisted of two structures: white matter (WM) and gray matter (GM). Realistic TACs' characteristic of ^{18}F-FDG were determined from human studies and assigned to WM and GM structures. The simulated imaging protocol lasted for 50 minutes: 4 frames of 30 s, 3 frames of 60 s, and 9 frames of 300 s. In total the phantom consisted of 16 time frames of data volumes with $128 \times 128 \times 47$ voxels of the size $2.25 \times 2.25 \times 2.43$ mm^3 per each frame. Fig. 1(a) shows a central transaxial plane of the phantom. Ground truth WM and GM TACs are presented in Fig. 1(b). A uniform attenuation map with attenuation coefficient 0.12 cm^{-1} was generated. We assumed that all the emitted counts except those attenuated were detected. To simulate the effect of attenuation correction, we first decorrected the noiseless projection data for attenuation by dividing them with the ACFs, and then generated the Poisson noise to the resulting projections. The noisy data was further weighted by the ACFs to account for the attenuation. The total number of counts $\sum_d \nu_{dt}$ in the last time frame was 9.98×10^6.

To model the errors introduced by image segmentation procedure, we consecutively applied a gray scale morphological dilation operator followed by erosion to the labelled image. The structuring elements for dilation and erosion were different. The spatial mismatches resulted in 30.4% and 29.5% of wrongly classified voxels for WM and GM, respectively. The accuracy of regional TACs reconstruction was measured using the average (over 10 noise realizations) root mean square (RMS) deviation of reconstructed TAC $\hat{\boldsymbol{\lambda}}_{\boldsymbol{k}}$ as a percentage of

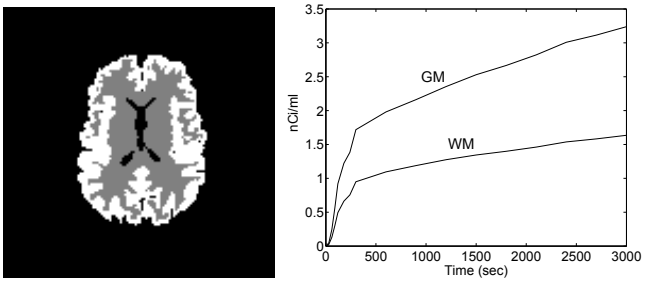

Fig. 1. (a) A central transaxial slice of the phantom. (b) Ground truth TACs for GM and WM structures.

the peak value from the ground truth TAC $\boldsymbol{\lambda}_k$

$$\sigma^{rms}(\hat{\boldsymbol{\lambda}}_k) = \frac{1}{N}\sum_n \frac{\sqrt{\frac{1}{T}\sum_t(\lambda_{kt}-\hat{\lambda}_{nkt})^2}}{\max_t \lambda_{kt}} \times 100\%, \quad (21)$$

where $\hat{\lambda}_{nkt}$ is the estimate of kth TAC at time interval t from noise realization $n = 1, \ldots, 10$.

^{18}F-FDG TACs were reconstructed from roughly labelled anatomical structures with the PML-EM algorithm based on ordinary Poisson approximation (PML-EM-OP) [4], and the PML-EM algorithm based on fixed multiplicative Poisson approximation (PML-EM-FMP). The regularization parameters were set to $\beta_d = 0.5 b_d^{\rm mask}/K\sum_{k,t}\lambda_{kt}^{(j+1)}, \gamma_k = 0.5 b_k^{\rm vol}\sum_t \lambda_{kt}^{(j+1)}$ for the PML-EM-OP and to $\beta_d = 0.5 b_d^{\rm mask}/(a_d K)\sum_{k,t}\lambda_{kt}^{(j+1)}$, $\gamma_k = 0.5 b_k^{\rm vol}/D\sum_{d,t}\lambda_{kt}^{(j+1)}/a_d$ for the PML-EM-PML. We assumed that the true proportions of different tissue types $b_k^{\rm vol}$ and the projections of a ground truth binary mask enclosing all the structures $b_d^{\rm mask}$ are known. Fig. 2 shows the convergence of σ^{rms} measure for WM and GM structures. After 40 iterations the PML-EM-FMP algorithm reduced the RMS error in reconstructed TACs to 0.41% and 0.18% for WM and GM, respectively. The PML-EM-OP method exhibited worse performance with σ^{rms} of 4.39% for WM and 1.86% for GM structure.

5. DISCUSSION

We presented an exact counting distribution to model the statistical behavior of emission tomography data pre-corrected for multiplicative correction factors. The proposed fixed multiplicative Poisson distribution is tractable, i.e does not contain infinite summations, that makes its use appealing for maximum -likelihood estimation problems. We applied accurate statistical data modeling for the task of ROI quantification in PET. We derived a joint penalized-likelihood estimator for TACs and ROIs from dynamic projection data pre-corrected for the effect of attenuation. The preliminary results demonstrated that for low count rates the modified PML-EM-FMP estimator based on fixed multiplicative Poisson approximation outperforms the PML-EM-OP one based on the ordinary

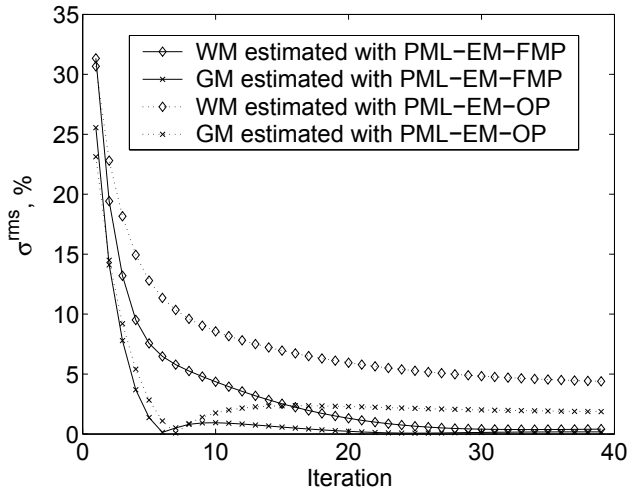

Fig. 2. Convergence of σ^{rms} measure versus iteration number for WM and GM structures. Forty iterations of PML-EM-OP and PML-EM-FMP algorithms.

Poisson approximation yielding lower RMS error for reconstructed TACs.

6. REFERENCES

[1] T. J. Herbert and R. Leahy, "Fast methods for including attenuation in the EM algorithm," *IEEE Trans. Nucl. Sci.*, vol. 37, no. 2, pp. 754–758, 1990.

[2] P. Kinahan, B. H. Hasegawa, and T. Beyer, "X-ray-based attenuation correction for PET/CT scanners," *Seminars Nucl. Med.*, vol. 33, pp. 166–179, 2003.

[3] C. Comtat, P. E. Kinahan, M. Defrise, C. Michel, and D. W. Townsend, "Fast reconstruction of 3D PET data with accurate statistical modeling," *IEEE Trans. Nucl. Sci.*, vol. 45, no. 3, pp. 754–758, 1998.

[4] E. Krestyannikov, J. Tohka, and U. Ruotsalainen, "Joint penalized-likelihood reconstruction of time activity curves and regions-of-interest from dynamic PET projection data," *IEEE Trans. Med. Imag.*, Submitted.

[5] M. C. Teich, "Role of doubly stochastic Neyman type-A and Thomas counting distributions in photon detection," *Appl. Opt.*, vol. 13, pp. 2457–2467, 1981.

[6] A. R. De Pierro, "On the relation between the ISRA and the EM algorithm for positron emission tomography," *IEEE Trans. Med. Imag.*, vol. 12, pp. 328–333, 1993.

[7] A. R. De Pierro, "A modefied expectation maximization algorithm for penalized likelihood estimation in emission tomography," *IEEE Trans. Med. Imag.*, vol. 14, pp. 132–137, 1995.